Raffel TR, Lloyd-Smith JO, Sessions SK, Hudson PJ, and Rohr JR. Does the early frog catch the worm? Disentangling potential drivers of a parasite age-intensity relationship in tadpoles.

Electronic Supplementary Material

Appendix 1: Estimation of tadpole ages

Tadpole age (i.e., days since initiation of hatching) was estimated from the mass of each tadpole using the temperature-dependent growth model of Berven et al. (1979):

$$ln\,(\Delta) = ln\,(\alpha) + \beta\, ln\,(T), \qquad (1)$$

where Δ is the developmental rate, α is a constant, T is the temperature in degrees C, and β is the temperature coefficient. We chose to use the growth rate model (grams/day) for age estimates rather than the differentiation model (developmental stages per day, Gosner 1960) because ranid tadpoles can halt development (but not growth) during certain times of the year independent of temperature (Crawshaw et al. 1992), and because the growth rate model explained the observed dichotomous masses of the stage 36 tadpoles (due to growth without differentiation over winter) whereas the differentiation model did not (Fig. S-1). Parameter values were obtained from Berven et al. (1979). Because the total number of degree days in a season at our site was intermediate between Berven et al.'s (1979) montane and lowland populations (approximately 887 degree-days for our pond using Berven et al.'s (1979) formula), we used the mean of the parameter values from the two populations (mass model: α = -12.8, β = 2.42; differentiation model: α = -18.9, β = 5.29). Larval age estimates based on these average parameters were similar to those calculated using parameter values from either montane (mass model: α = -11.4, β = 2.00) or lowland (mass model: α = -2.84, β = 2.84) populations and indicated that tadpoles over-winter at least once in this population, as expected for a pond with approximately 900 degree days per season (Fig. 1, Fig. S-1, Berven et al. 1979). Because the density of tadpoles in

terms of mass is approximately 1.0 g/mL (Skelly and Werner 1990), volume measurements of Berven et al. (1979) were assumed to be comparable to our mass measurements. Initial mass M_i (mass at onset of stage 25) was estimated by regressing mass vs. stage for early stage (25-28) tadpoles (N = 16, M_i = 0.046 g).

The models of Berven et al. (1979) only apply to the green frog larval period, which begins at stage 25 when the embryo completes its transition from dependence upon its yolk sac into a feeding tadpole (Duellman and Trueb 1986). However, hatching in green frogs occurs at approximately Gosner stage 19 (Schalk et al. 2002). Thus, tadpoles should be exposed to trematode infections during their last 5 "embryonic" stages, as well as during their larval stages. This post-hatching embryonic period was therefore added to the temperature-derived larval age (age since Gosner stage 25) of each tadpole. Data were unavailable for direct estimation of the length of the post-hatching embryonic period of green frogs, but leopard frogs take 6.9 days to complete this period at 18°C (Shumway 1940) and green frogs develop 19% slower as embryos than leopard frogs, at least during Gosner stages 1-19 (Moore 1939). This yielded an approximate post-hatching embryonic period of 8 days.

Average daily water temperatures were calculated using data collected every two hours from 6 March to 2 June of 2005 by a temperature logger (HOBO, Onset, Pocasset, MA) set 20 cm. below the water surface, and estimated for all other dates from 1 March 2004 to 1 November 2005 based on a strong correlation between air temperature (Bahrmann and Ayers 2005) and water temperature in State College PA, as described by Raffel et al. (2006).

Appendix 2: Probabilistic modeling of the age intensity curve

The cyst count for the environmental echinostomes represented cumulative exposure over the lifespan of each individual tadpole in the wild. For each individual, i, infection was assumed

to occur as an exponential process with a time-varying rate parameter, λ_i (t). In our most general model,

$$\lambda_i(t) = c\ \varepsilon(t)\sigma_i(t) \qquad (2)$$

where $\varepsilon(t)$ and $\sigma_i(t)$ are the relative seasonal exposure rate and relative susceptibility, respectively, of individual *i* on day *t*, and *c* is an unknown constant. The cumulative exposure over an individual's lifetime in the wild, from the date of emergence to the date of collection, is:

$$\lambda_{i,\text{tot}} = \int_{t_{emergence}}^{t_{collection}} c\ \varepsilon(t)\sigma_i(t)\,dt. \qquad (3)$$

Determination of the seasonal exposure rate $\varepsilon(t)$ was based on published data from surveys of echinostome-infected snail populations. No data were available on the seasonal abundance of echinostome cercariae for the pond from which these tadpoles were collected. However, the seasonal dynamics of relative echinostome abundance are similar across geographic regions (Sapp and Esch 1994; Schmidt and Fried 1997), and the relative level of exposure should be proportional to the abundance of infected snails, the first intermediate host of these echinostomes. Thus, we used the well-described seasonal infection dynamics of *P. trivolvis* snails (Sapp and Esch 1994; Wetzel and Esch 1996) as an index of the seasonal exposure of green frogs to echinostome cercariae at our site (Fig. 2A). Monthly estimates of snail abundance and infection prevalence were available except for the winter months, during which we assumed no exposure occurred since cold temperatures drive snails into the deep water or the substratum (Sapp and Esch 1994) and inhibit cercarial production (Lo and Lee 1996). For our modeling analysis, we required daily values of the relative exposure intensity, $\varepsilon(t)$, from the estimated emergence date of the oldest tadpole, 19-Jul-2004, to the date of capture, 14-Oct-2005. To estimate $\varepsilon(t)$, the monthly values were assumed to hold for the 15th day of each month, and

daily values were estimated by linear interpolation. The relative exposure intensity was assumed to be proportional to the product of snail abundance and the prevalence of cercarial shedding.

The relative susceptibility of tadpole i as a function of date, $\sigma_i(t)$, was derived from the relative susceptibility values for each developmental stage, $\sigma(s)$. $\sigma(s)$ was calculated using the quadratic fit of developmental stage to the arc-sine square-root transformed proportion of successfully encysted experimental trematodes (i.e., $\sin^{-1}(\sqrt{(\sigma(s_i))}) = \beta_0 + \beta_1(s_i) + \beta_2(s_i^2)$) and the estimates of the developmental stage of individual i as a function of calendar date, $s_i(t)$, using the temperature-dependent differentiation rate model of Berven et al. (1979) as described above. Tadpoles at stage 36 included the youngest second-year tadpoles and the oldest first-year tadpoles. In order to separate the animals which did over-winter from those that did not, the Gosner (1960) stage values of these tadpoles were adjusted by half a stage up or down, respectively. Because development ceases but growth continues during the winter (Crawshaw et al. 1992), the differentiation rate model slightly underestimated the ages of second-year tadpoles relative to the growth rate model under the original parameterization (Fig. S-1), so the stage-based and mass-based age estimates were brought into agreement by minor adjustment of the alpha parameter from -18.9 to -19.3 (Fig. S-1). The range of developmental stages in the experimental infection data (26-39) was smaller than the range needed to parameterize the exposure model (19-39), so the susceptibility value for developmental stage 26 was used for all stages ≤ 26. The results of model selection were robust to changes in this assumption.

We tested five models for this infection process, which include increasing degrees of covariate information. In the null model of constant exposure rate, exposure and susceptibility were fixed through time so values of $\lambda_{i,\text{tot}}$ scale linearly with tadpole age at capture. More complex models incorporated stage-dependent susceptibility $\sigma_i(t)$, seasonal variation in exposure $\varepsilon(t)$, or both. In models for which susceptibility or exposure did not vary through time, ε and σ in

Equation (3) were set to the mean values of $\varepsilon(t)$ and $\sigma(s)$ respectively. Because $\varepsilon(t)$ and $\sigma_i(t)$ are completely specified by independent data, all models for $\lambda_{i,\mathrm{tot}}$ have one free parameter, c.

These models were fit to the observed cyst counts using maximum likelihood methods, i.e., for each model the free parameter(s) θ were varied to maximize the log-likelihood

$$\boldsymbol{L} = \log\left[\prod_{i=1}^{N} \boldsymbol{f}\left(\boldsymbol{y}_i|\theta\right)\right]$$

where y_i is the count of environmental cysts, $N = 92$ is the number of tadpoles for which environmental cyst counts were available, $f(y)$ is the probability density function of the probability distribution, and θ represents the free parameters of the model. Because the parasite intensities were overdispersed, the data were modeled using a negative binomial distribution with intensity $\lambda_{i,\mathrm{tot}}$ and free dispersion parameter, k. Optimization was conducted using the multi-dimensional constrained optimization function "fminsearchbnd" (available on the Matlab Central file exchange at http://www.mathworks.com/matlabcentral/) in Matlab v6.1 (Mathworks, Cambridge MA).

Model selection was conducted using Akaike's information criterion, AIC = $-2\,L + 2\,K$, where K is the number of free parameters in the model. The AIC values were rescaled by subtracting the minimum score, yielding ΔAIC scores. Akaike weights, w_i, were then calculated for each of the candidate models:

$$\boldsymbol{w_i} = \frac{\exp\left(-\frac{1}{2}\Delta\mathbf{AIC}_i\right)}{\sum_{j=1}^{5}\exp\left(-\frac{1}{2}\Delta\mathbf{AIC}_j\right)}.$$

The Akaike weight w_i can be interpreted informally as the approximate probability that model i is the best model of the set of candidate models considered, indicating accurate representation of the information in the data with a parsimonious number of parameters (Burnham and Anderson 2002).

The robustness of these results to our limited sample size was investigated using a bootstrapping analysis. The observed dataset was sampled 10,000 times with replacement and the Akaike weight calculated for each of the four candidate models, to determine the frequency with which each of the four models was selected. The mean and median Akaike weights mirrored the weights reported in Table 2. The results indicate clearly that our results are not influenced by the specific composition of the data set.

Appendix 3: Modeling the effect of hatching date on trematode burden at metamorphosis

To predict how hatching date influences the total trematode burden of a frog at metamorphosis, the larval period (days to metamorphosis) for a tadpole hatched on a given date in Beaver 1 pond was estimated using the degree-day model of Berven et al. (1979) and cumulative exposure through metamorphosis was calculated assuming seasonal exposure as shown in Fig. 2A. The degree day model of Berven et al. (1979) is:

$$L(T - \alpha) = K,$$

where L is the larval period in days, T is temperature in degrees Celsius, α is the temperature below which development does not take place and K is the total number of degree-days required for metamorphosis (degree day = one degree of temperature above the developmental zero for a period of one day). Parameters α and K were again estimated based on the average Berven et al.'s (1979) montane and lowland populations (α = 15.56°C; K = 1008 degree-days), and daily pond temperatures were estimated as described in Appendix S-1. The number of days required for metamorphosis (L) for a tadpole hatching on a given date h was estimated using the following equation:

$$\sum_{i=h}^{h+:L} (T_i - \alpha) = K\,.$$

Daily exposure to trematodes was estimated using interpolated seasonal exposure rates as described above, and cumulative exposure to trematodes was estimated by summing daily exposure rates across the larval period. Stage-dependent susceptibility was excluded from this model because it was found to be unimportant in the age-intensity analysis. To simulate climatic warming/cooling or latitudinal variation in temperature, the entire annual pond temperature profile was uniformly raised or lowered in 1-degree increments up 6°C and down 3°C. This approximated the expected temperature range across the geographic range of *R. clamitans* (35-45°N and 70-95°W, Conant and Collins 1998), based on average temperatures in this region for the years 1993-2002 (the most recent 10 years available at the time of the analyses). Regional temperature data were obtained from the Climate Research Unit (CRU TS 2.1) dataset, University of East Anglia, available at http://www.cru.uea.ac.uk/ (Mitchell and Jones 2005). An increase of 6°C also approximates the predicted change in temperature for North America over the next century, given a worst-case scenario of high population growth, slow economic development and slow technological change (IPCC 2007). This model makes the simplifying assumptions that seasonal exposure rates are invariant with respect to average temperature and that the number of degree days needed to metamorphose (K) is constant across green frog populations.

Appendix 4: Simulation analysis to rule out small sample size effects

Small sample sizes can lead to underestimation of mean intensity for aggregated distributions of parasites (Gregory and Woolhouse 1993). This means that the small sample size of second-year tadpoles could have led to underestimation of parasite intensity in older tadpoles and a false indication of a curvilinear age-intensity relationship (i.e., the significant quadratic effect of exposure time on intensity). We therefore conducted a simulation analysis to confirm

that the observed parasite intensities for second-year tadpoles were indeed lower than expected under the null model of a linear age-intensity relationship. Our sample size for first-year animals was much larger than for second-year animals and thus should provide more reliable intensity estimates. Hence, we used the null model of a linear fit for the relationship between exposure time and intensity for the first-year tadpoles to estimate the null expectation for the intensity of larval echinostomes in the second-year tadpoles, using a negative binomial generalized linear model (glm) with a log link. To ensure that our analyses were conservative, we used the lower 95% confidence limit around this intensity estimate because it was closer to the observed second-year tadpole parasite intensities. In our simulation, we replaced the parasite intensity data for the eight second-year tadpoles with eight parasite intensities selected randomly from a negative binomial distribution with a mean equivalent to the lower 95% confidence limit just described and theta equal to theta of the glm for the first-year tadpoles. We then fit a quadratic negative binomial glm on the full age-intensity dataset (including the original data for first-year tadpoles and the simulated data for second-year tadpoles). We repeated this procedure 10,000 times to determine the proportion of simulations that produced quadratic coefficients that were at least as negative as the quadratic coefficient for the observed relationship. Only 2.01% of simulations yielded quadratic coefficients as negative as that observed for the real data, even under these conservative assumptions.

Appendix 5: Analyzing residuals from probabilistic models

Model selection using the Akaike information criterion only yields conclusions about the relative support for models in the candidate set of models under consideration. Just because one of the probabilistic models (i.e., seasonal exposure) fits the data better than the others does not necessarily indicate that it fully explains the curvature of the age-intensity relationship. To

determine whether curvature remained after fitting probabilistic models to the data, we tested for significant curvature and linear trends in the residuals from these models. The residuals were log-transformed to improve normality, following addition of a constant to ensure that all values were positive. The adjusted and transformed residuals were given by $r_{i,\mathrm{adj}} = \log[(r_i - r_{\min}) + 1]$, where $r_{\min} < 0$ is the minimum value of all residuals for a given model. The adjusted residuals were regressed against age using linear and quadratic functions. Because of the complexity of our model and the non-conventional transformation applied to the residuals, we evaluated the results of these regressions using a third bootstrap analysis (Efron and Tibshirani 1994). For each candidate model, 1000 replicate datasets were simulated by generating negative binomial random variates with means equal to $\lambda_{i,\mathrm{tot}}$ for the model in question, and dispersion parameters k equal to the maximum likelihood estimate derived from fitting the true data. By fitting the negative binomial model to each of these simulated data sets, and analyzing the residuals as described above, the sampling distributions and p-values for the regression parameters could be determined.

Log-residuals from all models exhibited significant negative slopes when regressed against age. We hypothesized that this pattern arose because negative binomial models generate predominantly negative residuals from aggregated data, and the degree of aggregation increased with age. To test this hypothesis, and to ensure that these trends did not arise because the model failed to predict the intensity of infection in older tadpoles, we applied a fourth bootstrap analysis to assess the distribution of slopes derived from data sets simulated from the negative binomial models. From this analysis, the linear slopes of these residuals were lower than expected for the null model (P = 0.038; Fig. S-4A) and the model with stage-dependent susceptibility (P = 0.051; Fig. S-4B), but were not significantly different from the expected trends for either of the models with seasonal exposure (both P > 0.15; Fig. S-4C, S-4D). This result confirmed that the negative

residual slopes were caused by properties of the negative binomial distribution, indicating that there was no significant signal in the data beyond that explained by seasonal exposure. It is worth noting that there was no correlation between the residuals from these best-fit models and numbers of experimental cysts ($P > 0.3$), further confirming the lack of interaction between the two echinostome species.

References

Bahrmann C, Ayers B (2005) State College Hourly Weather Data 1-Jun-2004 to 1-Nov-2005. Pennsylvania Department of Environmental Protection. Accessed 1-Nov-2006. http://climate.psu.edu/data/mesonet/datainv.php.

Berven KA, Gill DE, Smithgill SJ (1979) Countergradient selection in the green frog, *Rana clamitans*. Evolution 33:609-623

Burnham KP, Anderson DR (2002) Model selection and multimodel inference: a practical information-theoretic approach. Springer, New York

Conant R, Collins JT (1998) A field guide to reptiles and amphibians: Eastern and central North America, 3rd edn. Houghton Mifflin, New York

Crawshaw LI, Rausch RN, Wollmuth LP, Bauer EJ (1992) Seasonal rhythms of development and temperature selection in larval bullfrogs, *Rana catesbeiana* Shaw. Physiol Zool 65:346-359

Duellman WE, Trueb L (1986) Biology of Amphibians. The Johns Hopkins University Press, Baltimore

Efron B, Tibshirani RJ (1994) An introduction to the bootstrap. Chapman and Hall, London

Gosner KL (1960) A simplified table for staging anuran embryos and larvae with notes on identification. Herpetologica 16:183-190

Gregory RD, Woolhouse MEJ (1993) Quantification of parasite aggregation: a simulation study. Acta Trop 54:131-139

IPCC (2007) Climate change 2007: Synthesis report. Contribution of working groups I, II and III to the fourth assessment report of the Intergovernmental Panel on Climate Change. In: team Cw, Pachauri RK, Reisinger A (eds). IPCC, Geneva, Switzerland, p 104

Lo CT, Lee KM (1996) Pattern of emergence and the effects of temperature and light on the emergence and survival of heterophyid cercariae (*Centrocestus formosanus* and *Haplorchis pumilio*). J Parasitol 82:347-350

Mitchell TD, Jones PD (2005) An improved method of constructing a database of monthly climate observations and associated high-resolution grids. Int J Climatol 25:693-712

Moore JA (1939) Temperature tolerance and rates of development in the eggs of Amphibia. Ecology 20:459-478

Raffel TR, Hoverman JT, Halstead NT, Michel PJ, Rohr JR (in press) Parasitism in a community context: Trait-mediated interactions with competition and predation. Ecology

Raffel TR, Rohr JR, Kiesecker JM, Hudson PJ (2006) Negative effects of changing temperature on amphibian immunity under field conditions. Funct Ecol 20:819-828

Sapp KK, Esch GW (1994) The effects of spatial and temporal heterogeneity as structuring forces for parasite communities in *Helisoma anceps* and *Physa gyrina*. Am Midl Nat 132:91-103

Schalk G, Forbes MR, Weatherhead PJ (2002) Developmental plasticity and growth rates of green frog (*Rana clamitans*) embryos and tadpoles in relation to a leech (*Macrobdella decora*) predator. Copeia 2002:445-449

Schmidt KA, Fried B (1997) Prevalence of larval trematodes in *Helisoma trivolvis* (Gastropoda) from a farm pond in Northampton County, PA with special emphasis on *Echinostoma trivolvis* (Trematoda) cercariae. J Helminthol Soc W 64:157-159

Shumway W (1940) Stages in the normal development of *Rana pipiens*. Anat Rec 78:139-147

Skelly DK, Werner EE (1990) Behavioral and life-historical responses of larval *American toads* to an odonate predator. Ecology 71:2313-2322

Wetzel EJ, Esch GW (1996) Seasonal population dynamics of *Halipegus occidualis* and *Halipegus eccentricus* (Digenea: Hemiuridae) in their amphibian host, *Rana clamitans*. J Parasitol 82:414-422

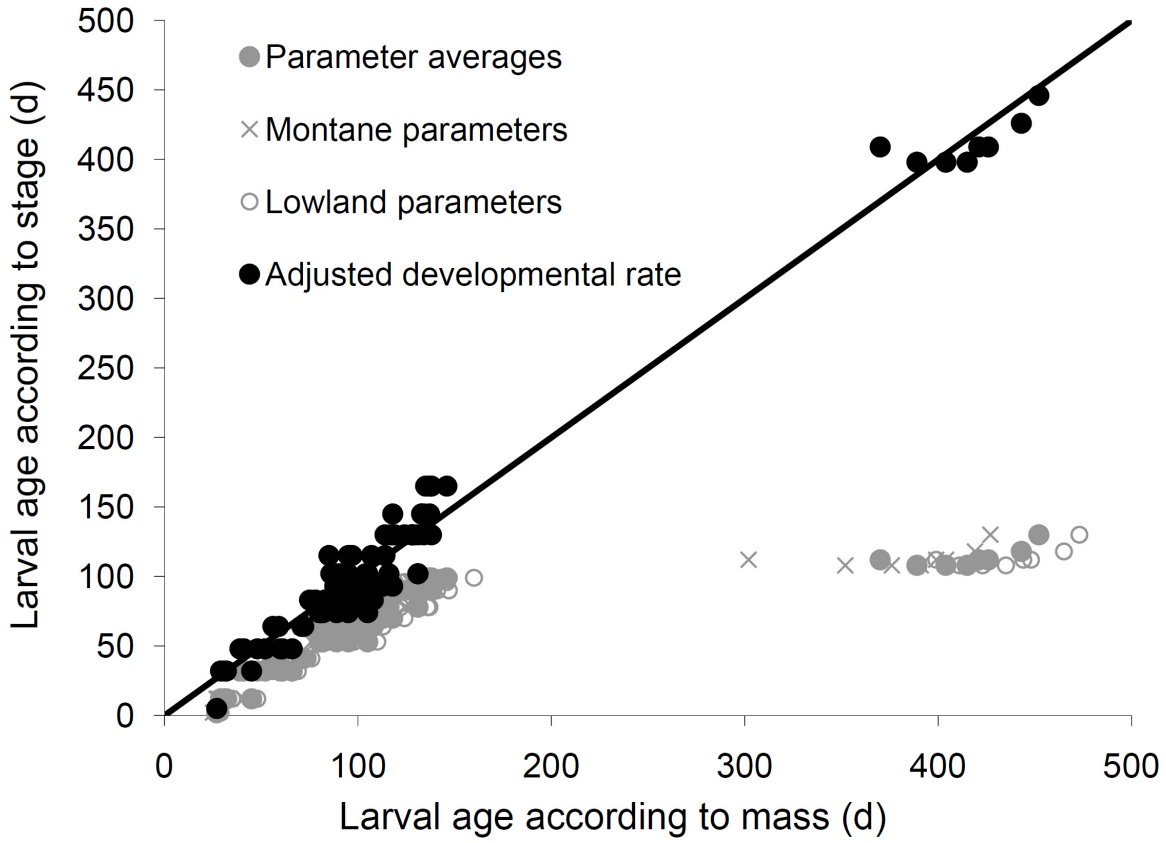

Figure S-1: Differences in age estimates calculated using the temperature-dependent growth rate model (larval age according to mass) compared to the temperature-dependent developmental rate model (larval age according to stage). The growth rate model estimates were insensitive to the values of the model parameters, yielding a similar dichotomy between first- and second-year tadpoles regardless of whether parameter estimates were taken from montane or lowland populations.

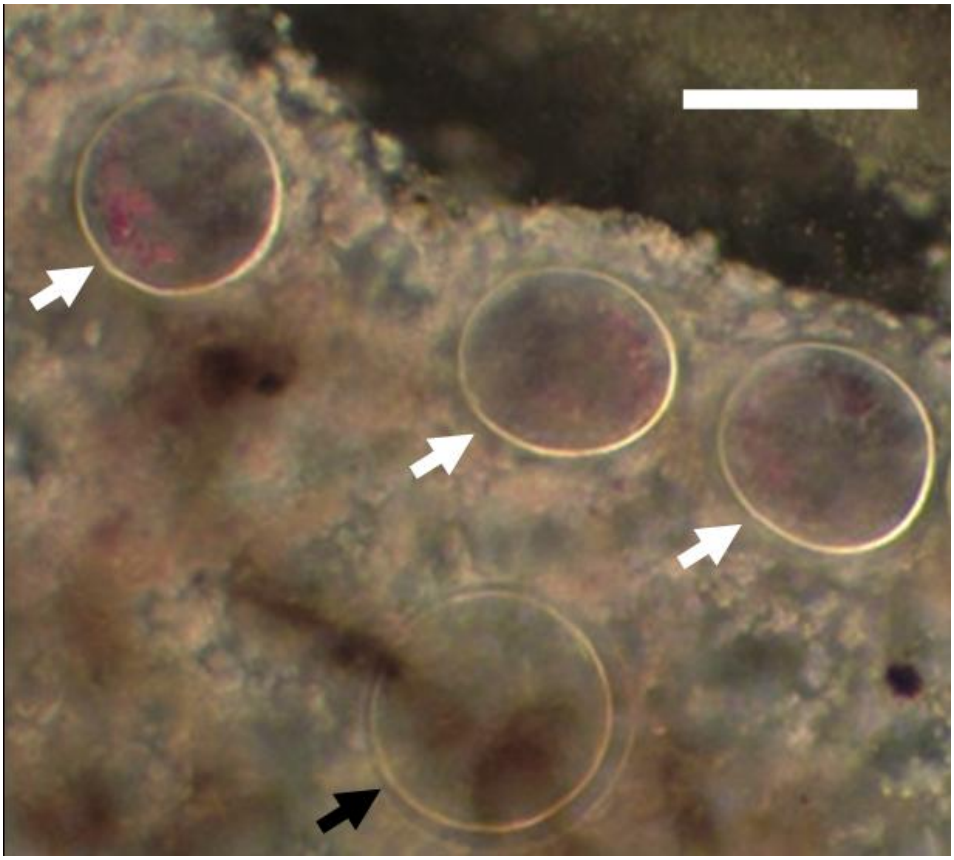

Figure S-2: Photomicrograph comparing experimental cysts (white arrows) with a single environmental cyst (black arrow). Scale bar = 100 μm.

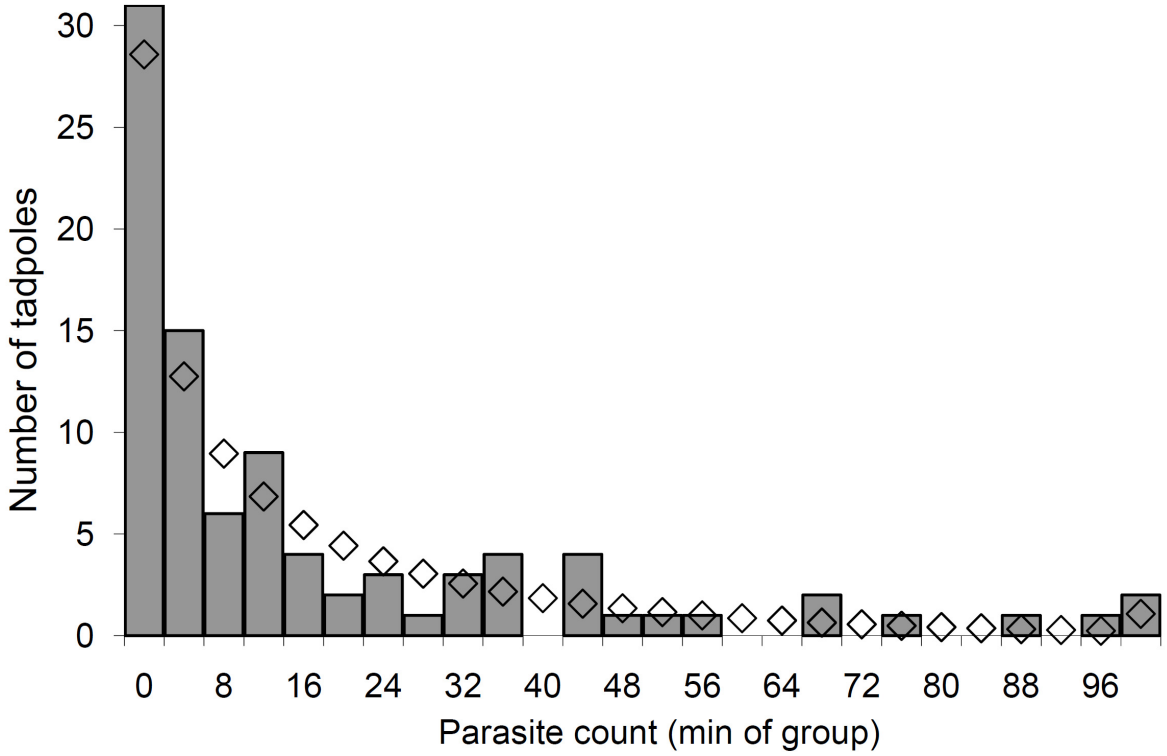

Figure S-3: Aggregated distribution pattern of naturally occurring echinostome cysts in this population of green frog tadpoles. The open diamonds indicate the expected values for a best-fit negative binomial distribution with k = 0.57.

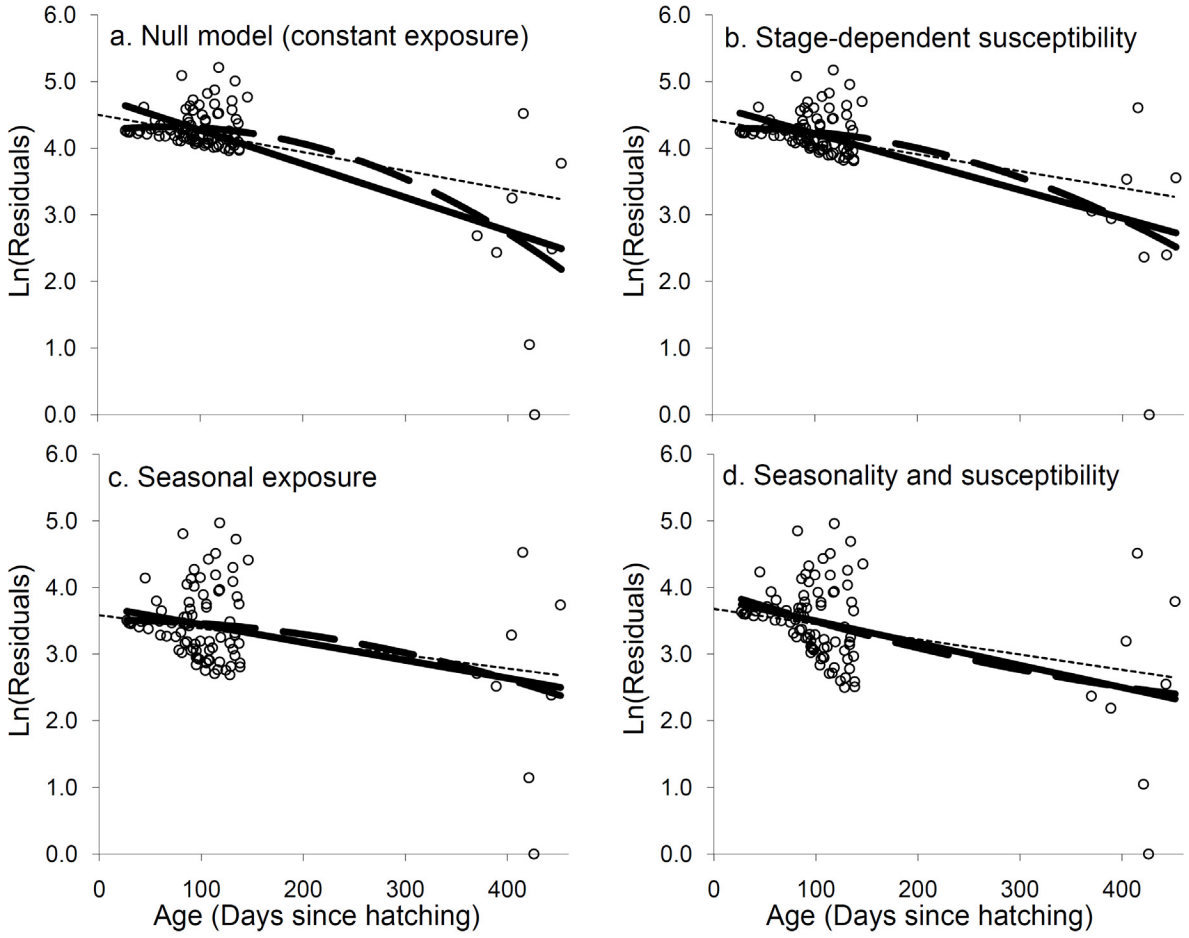

Figure S-4: Residual trends for (A) the null model of constant exposure, compared to models incorporating (B, D) stage-dependent susceptibility and (C, D) seasonal exposure. Residuals were log-transformed to improve normality (see Methods). The best-fit linear (thick solid line), quadratic (thick dashed line) fits to these residuals, and the expected trend based on bootstrap analysis (narrow dashed line), are shown on each graph. All 4 models result in negative trends in the residuals, but this is to be expected since aggregated data yields predominantly negative residuals in negative binomial models and the degree of aggregation increased with age.

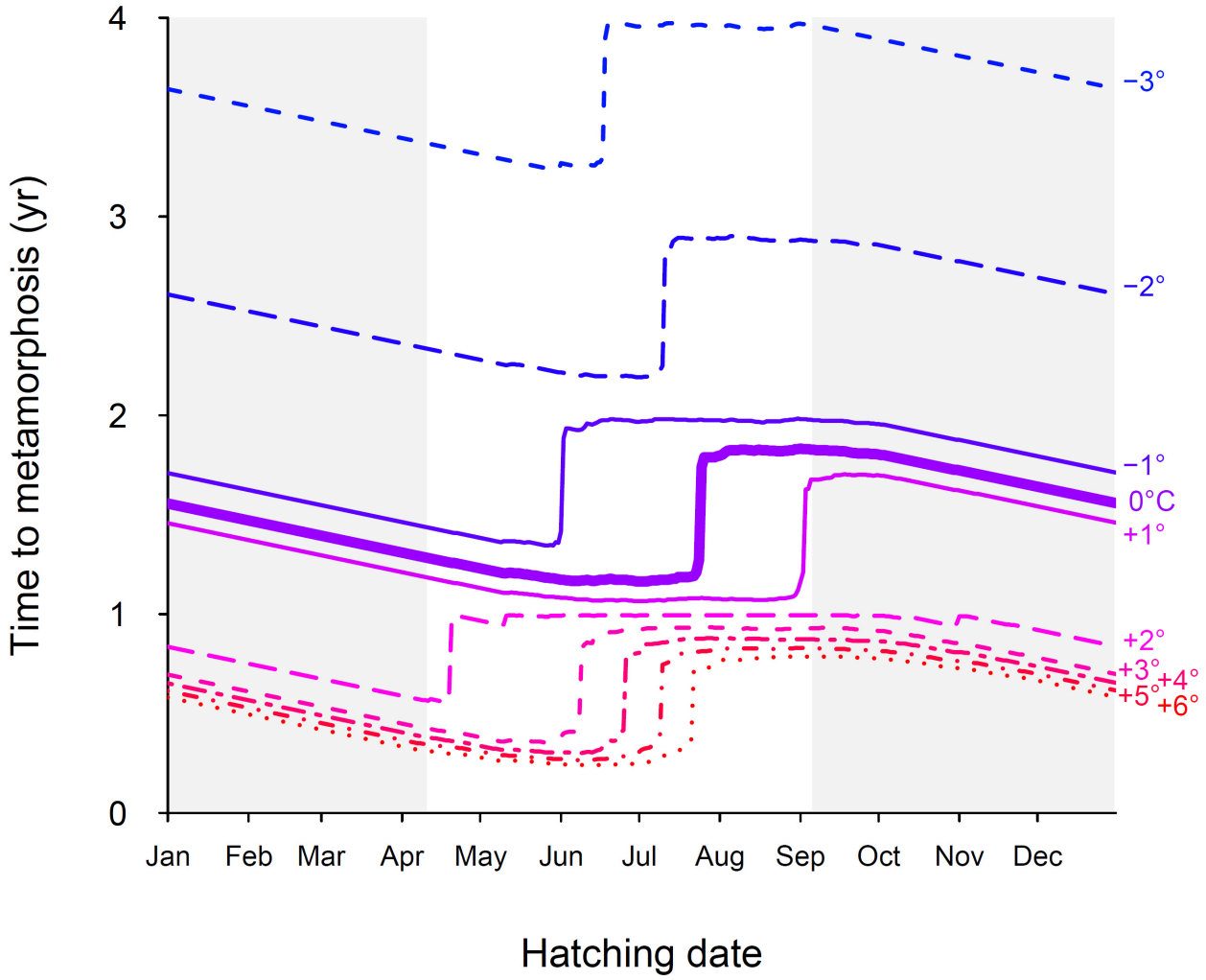

Figure S-5: Predicted time to metamorphosis (larval period, *L*) of a green frog (*Rana clamitans*) tadpole hatching on a given date, based on the degree day model of Berven et al. (1979). The model output using the Beaver 1 pond temperature profile (0°C) is indicated by a bold solid line, and narrower (solid, dashed or dotted) lines indicate model outputs given simulated warming (+1 to +6°C) or cooling (-1 to -3°C). Gray shading indicates the period outside the known green frog breeding season